Available online at www.sciencedirect.com
ScienceDirect
Dyes and Pigments 76 (2008) 179–186
DYES and PIGMENTS
www.elsevier.com/locate/dyepig

Gray–blue Al_2O_3–MoO_x ceramic pigments: Crystal structure, colouring mechanism and performance

Michele Dondi [a], Francesco Matteucci [a,*], Giovanni Baldi [b], Andrea Barzanti [b], Giuseppe Cruciani [c], Isabella Zama [a], Claudia L. Bianchi [d]

[a] *ISTEC-CNR, Institute of Science and Technology for Ceramics, Via Granarolo 64, 48018 Faenza, Italy*
[b] *CE.RI.COL., Colorobbia Research Centre, Via Pietramarina 53, 50053 Sovigliana-Vinci (Fi), Italy*
[c] *Department of Earth Sciences, University of Ferrara, Via Saragat 1, 44100 Ferrara, Italy*
[d] *Department of Physical Chemistry & Electrochemistry, University of Milan, Via Golgi 19, 20133 Milano, Italy*

Received 21 February 2006; received in revised form 16 April 2006; accepted 9 August 2006
Available online 10 October 2006

Abstract

Grayish-blue coloured alumina–molybdena was synthesized by high temperature reducing firing and experimented as ceramic pigment. Synchrotron light and conventional X-ray diffraction powder, ICP-OES and BET analyses proved that molybdenum spreads over alumina surface, without entering the corundum lattice, with a high superficial concentration (i.e. 27–99 Mo atoms nm^{-2}) implying a prevailing octahedral coordination and a certain long-range order, eventually resulting in the formation of crystalline MoO_2. XPS and DRS suggested the occurrence of different valences, Mo(VI) being predominant over Mo(V) and Mo(IV). The colouring mechanism is mainly due to electronic absorption of Mo(V) in the red–orange region of the visible spectrum, giving rise to a characteristic blue shade; the gray cast is caused by extensive light absorption by Mo(IV) crystal field transitions and particularly Mo–O charge transfer. The colouring performance of Al_2O_3–MoO_x in ceramic glazes and porcelain stoneware bodies for wall and floor tiles is excellent, being equivalent to the pigment coloration. Thermal stability in these matrices seems to be mostly affected by Na_2O and MgO. However, the distinctly blue shade of these pigments is much less intense than that of the most performant ceramic colorants. At all events, alumina–molybdena system develops a peculiar colour that cannot be reproduced unless utilising the most expensive blue and black cobalt-bearing ceramic pigments.

Keywords: Ceramic pigments; Colouring performance; Molybdenum oxides; Optical properties

1. Introduction

The Al_2O_3–MoO_3 system has attracted a noteworthy interest, in the last decade, for its catalytic properties and its potential applications in a great deal of reactions, especially hydrodesulfurization, ethylene polymerization and isomerization [1,2]. Hence, alumina–molybdena interactions have been thoroughly investigated, with special emphasis on adhesion mechanisms and kinetics, valences and coordination of Mo ions, short-range and long-range order of Mo oxide, formation of transient phases, effect of additives and conditions of thermal treatment [2–12].

The adhesion of Mo on the surface of α-Al_2O_3 occurs by chemical adsorption, with no cationic substitution into the crystal lattice of corundum [2–7]. During the thermal treatment, Mo spreads onto the alumina by a diffusion mechanism involving probably both surface and gas phase transport by sublimation–crystallization of molybdenum oxide [5,6].

Molybdena changes coordination and long-range order depending on its superficial concentration on α-Al_2O_3: for very low concentrations (<5.6 Mo atoms nm^{-2}) highly dispersed tetrahedral [MoO_4] sites are present; above this

* Corresponding author. Tel.: +39 0 546 699738; fax: +39 0 546 46381.
E-mail address: matteucci@istec.cnr.it (F. Matteucci).

0143-7208/$ - see front matter © 2006 Elsevier Ltd. All rights reserved.
doi:10.1016/j.dyepig.2006.08.021

dispersion limit, there are tetrahedral and octahedral sites co-existing; for high concentrations, a long-range ordering of $[MoO_6]$ occurs, giving eventually rise to crystalline MoO_3 or MoO_2 in reducing conditions [2–4,7].

On the corundum surface, Mo ions occur mainly with valence (VI), as detected by XPS, even after a thermal cycle in reducing conditions. However, the occurrence of lower valences of molybdenum is somehow evidenced by optical spectroscopy; as a matter of fact, many Al_2O_3–MoO_3 products prepared in reducing environment exhibit a grayish-blue shade that is not consistent with the presence of Mo(VI) only [13,14].

The possibility to obtain heat-resistant, blue-coloured oxides is of the highest interest for the ceramic industry, as all the ceramic pigments in the market contain cobalt (e.g. Co_2SiO_4, $CoAl_2O_4$, $(Zn,Co)SiO_4$) [15,16] and there are growing problems concerning the toxicity, high cost and limited availability of cobalt oxide [16]. On the other hand, the widely used V–$ZrSiO_4$ pigment is turquoise and cannot impart a pure blue coloration to ceramic wares [15].

Assessing the potential of alumina–molybdena as ceramic pigment is the main goal of the present work. For this purpose, Al_2O_3–MoO_x powders were synthesized in industrial-like conditions, characterised from the structural and spectroscopic viewpoints, then tested in several ceramic applications (wall and floor tiles, sanitary ware) in a wide range of temperature (950–1300 °C).

2. Materials and methods

2.1. Sample preparation

Three samples were prepared by dry mixing Al_2O_3 and MoO_3, with 99.9% of purity and particle size distribution of 20–30 μm, in the following Al_2O_3/MoO_3 weight ratios: 92:8 (AM8), 90:10 (AM10) and 85:15 (AM15). Mixtures were fired in reducing atmosphere in a mullite crucible up to 1300 °C with a heating rate of 5 °C min^{-1}, 2 h of soaking time (permanence at the maximum firing temperature) and natural cooling. The reducing atmosphere in the kiln was obtained by fluxing nitrogen/hydrogen in the 95:5 ratio up to 200 °C through a pine hole in the bottom of the crucible, so that the sample was crossed by gas. After firing the powders were wet milled, dried and sieved at 100 microns.

2.2. Sample characterisation

Laboratory X-ray powder diffraction data were collected on a Philips PW 1820/00 diffractometer at room temperature (Cu Kα radiation; 15–130° 2θ range; $\Delta 2\theta$ step 0.02°; counting time per step 10 s; diffracted-beam graphite monochromator) on the samples AM10 and AM15. In order to determine accurately the crystal structure parameters, the sample AM8 was characterised through high resolution X-ray powder diffraction, performed at the Swiss–Norwegian Beam Line (ESRF, Grenoble, France). Powder samples, filled in glass capillaries of 0.5 mm, were mounted in the Debye–Scherrer geometry ($\lambda = 0.79982$ Å, 1–52.5° 2θ range; $\Delta 2\theta$ step 0.0025°; counting time per step 1.5 s). Crystal structure Rietveld refinements were performed using the GSAS-EXPGUI [17,18] package (see Table 1). Starting atomic parameters for the corundum were taken from Maslen [19], adopting the same *R-3cH* space group. The number of independent refined variables ranged up to 24: scaling factors, zero-point correction, cell dimensions, 6–12 coefficients of the shifted Chebyschev function to fit the background, atomic positions, and profile coefficients (one Gaussian GW and two Lorentzian terms $[L_x,L_y]$). The Al vs. Mo fraction in the cationic site was refined by contrasting their X-ray scattering curves and assuming full occupancy of the cationic site. Refined unit cell parameters and crystallographic details are given in Table 1. X-ray photoelectron spectra were taken in a M-probe apparatus (Surface Science Instruments). The source was monochromatic Al K radiation (1486.6 eV). A spot size of 200×750 μm and a pass energy of 25 eV were used. The energy scale was calibrated with reference to the $4f_{7/2}$ level of a freshly evaporated gold sample, at 84.0 ± 0.1 eV, and with reference to the $2p_{3/2}$ and 3s levels of copper at 932.5 ± 0.1 and 122.39 ± 0.15 eV, respectively. The binding energies (BE) were corrected for specimen charging by referencing the C 1s peak to 284.6 eV, and the background was subtracted using Shirley's method. The C region was fitted into two or three peaks, depending on the tail shape. The deconvolution was performed using only Gaussian line shapes. The accuracy of the reported BE can be estimated to be ±0.1 eV. With a monochromatic source, an electron flood gun is required to compensate the build up of positive charge on the samples during the analyses, when insulating samples are analyzed: a value of 5 eV has been selected. UV–vis–NIR spectroscopy was performed by diffuse reflectance with a $BaSO_4$ integrating sphere (Perkin Elmer λ35) in the 300–1100 nm range, step 0.3 nm, using $BaSO_4$ as a reference. Energy and width of the main absorbance peaks in the optical spectra were determined using Gaussian bands for *d–d* transitions and Lorentzian bands for Mo–O charge transfer through a deconvolution procedure (PFM, OriginLab). Microstructural analysis was carried out by scanning electron microscopy (SEM, Cambridge 360, Oxford, UK). Measurement of specific surface of pigments was performed by nitrogen adsorption with single point method using a Micromeritics FlowSorb II 2300 apparatus (ASTM C 1069), while the amount of molybdenum was determined by inductively coupled plasma emission spectrophotometry (ICP-OES) with a Varian Liberty 200 equipment; the analytical solutions were obtained by melting with lithium tetraborate at 1200 °C in graphite crucible. The surface concentration of Mo was estimated based on ICP-OES and BET data according to Ref. [3]. The colouring performance was appraised by adding the pigment AM10 (5 wt%) to a ceramic body and to three glazes for porcelain stoneware (G1) and stoneware tiles (G2 and G3) that underwent firing in industrial kilns at temperatures between 1150 and 1220 °C. Moreover, thermal stability was appraised by wet mixing the alumina–molybdena pigments (5 wt%) into several ceramic matrices: two glassy coatings (F1 and F2)

Table 1
Crystal structure and chemical composition of alumina–molybdena pigments

	Unit	AM8	AM8	AM10	AM15	Corundum	Corundum
Source		SLD	LXRD	LXRD	LXRD	ICSD73724	ICSD31546
Observations	1	47	98	98	98	–	–
R_{Bragg}	1	0.04	0.05	0.05	0.04	–	–
R_{wp}	1	0.07	0.17	0.16	0.16	–	–
α-Al_2O_3	wt%	100	100	100	99.1(2)	100	100
MoO_2	wt%	0	0	0	0.9(2)	0	0
Unit-cell *a*	Å	4.7598(1)	4.761(1)	4.761(1)	4.761(1)	4.7540(5)	4.7586(1)
Unit-cell *c*	Å	12.9943(1)	12.997(3)	12.997(3)	12.999(1)	12.9820(6)	12.9906(1)
Unit-cell volume	$Å^3$	254.957	255.13	255.14	255.22	254.09	254.75
Al–O_1 distance	Å	1.9714(4)	1.972(1)	1.974(1)	1.973(1)	1.9699	1.970
Al–O_2 distance	Å	1.8551(2)	1.855(1)	1.855(2)	1.855(2)	1.8525	1.855
z (Al)	1	0.3521(1)	0.352(1)	0.352(1)	0.352(1)	0.3522(1)	0.3520(1)
x (O)	1	0.6937(2)	0.694(1)	0.694(1)	0.693(2)	0.6938(2)	0.6936(3)
Al occupancy	1	1.01(1)	1.01(2)	1.01(2)	1.01(2)	–	–
MoO_3 content	mg g^{-1}	–	7.3	13.4	24.9	–	–
I_{Mo}/I_{Al} by XPS	1	–	0.91	1.02	1.20	–	–
Specific surface	m^2 g^{-1}	–	1.12	0.71	1.05	–	–
Surface concentration	Mo atoms nm^{-2}	–	27.3	79.0	99.2	–	–

Note: SLD: Synchrotron light radiation; LXRD: Laboratory X-ray powder diffraction. Figures in parentheses are standard deviations in the last decimal figure. R_{Bragg} is referred only to corundum reflections. The number of reflections is referred to corundum ones. Isotropic displacement parameters were first refined then kept fixed in the final refinement cycles.

and four glazes (S1 to S4), whose chemical composition and main physical properties are reported elsewhere [20]. Later on, the slurry was sprinkled over a ceramic substrate that was further fired in an electric laboratory kiln at different temperatures from 950 to 1300 °C (45–60 min cold-to-cold, 5–10 min annealing) depending on the glaze. Colour was determined by optical spectroscopy (Hunterlab MSXP 4000) expressing the results as CIE L^*, a^* and b^* parameters, where L^* is a measure of brightness (100 = white, 0 = black) while a^* and b^* of chroma ($-a^*$ = green, $+a^*$ = red, $-b^*$ = blue, $+b^*$ = yellow). The effect of the chemical composition of glazes and glassy coatings on thermal stability of pigments was evaluated by a multivariate statistical analysis, applying the extraction of principal components using the StatSoft Statistica software.

3. Results and discussion

3.1. Chemical and physical characteristics

Alumina–molybdena pigments are constituted by euhedral, prismatic to tabular corundum crystallites with a particle size distribution mainly between 2 and 10 μm (Fig. 1). The specific surface area is very low, approximately 1 m^2 g^{-1} (Table 1). There is no evidence of individual particles of molybdenum oxide by EDS microprobe analyses.

The high temperature of industrial-like synthesis caused a relevant volatilisation of molybdenum, as the actual MoO_3 contents of pigments range from 0.7 to 2.5 wt% as measured by ICP-OES. The corresponding surface concentration is between 27 and 99 Mo atoms nm^{-2} (Table 1). We are dealing with remarkably high values, that are largely exceeding the dispersion limit of molybdenum on corundum surfaces, estimated to be around 5–6 atoms nm^{-2}. This circumstance implies that Mo ions are expected to be mostly coordinated by six oxygens, having also a certain degree of long-range order of [MoO_6] octahedra [2–4,7].

3.2. Conventional and synchrotron X-ray diffraction

Corundum is the only crystalline phase detected by X-ray diffraction in the pigment samples AM8 and AM10. A tiny amount of tugarinovite (MoO_2) was also found in sample AM15. Actually, there are some indications for the occurrence of further molybdenum phases, as suggested by very weak and

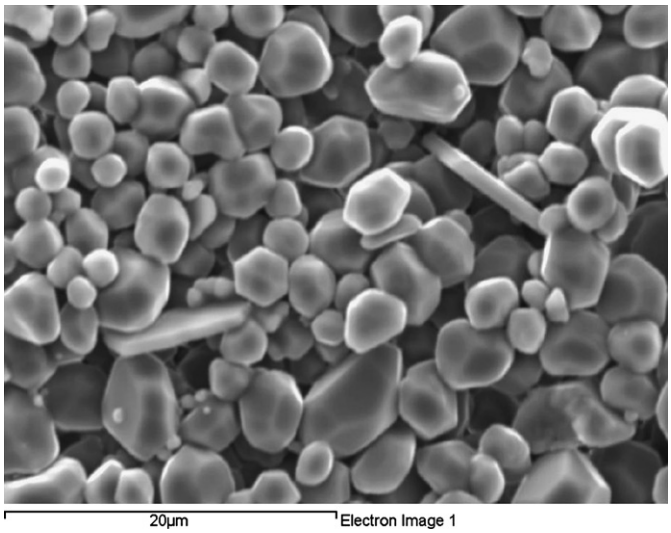

Fig. 1. Scanning electron micrograph of the pigment AM10.

broad peaks (Fig. 2) tentatively attributable to MoO_3 or to a mixed valence oxide (Mo_4O_{11}), but it was not possible to solve them.

The Rietveld refinement of the corundum structure gave reliable results for both conventional and synchrotron X-ray diffraction data (Fig. 3). The refined crystallographic parameters for all the three samples do not exhibit any significant variation by varying the molybdenum doping amount (Table 1). The cell parameters of the doped alumina pigments are slightly larger than those of the undoped structure [19] being within the range of the pure α-Al_2O_3 [21] due to different processing conditions (i.e. raw materials, firing cycle, etc.). The cell parameters and refined octahedral distances in doped samples are larger than those reported for the undoped structure; this could be interpreted as caused by the isomorphous substitution of Mo ions for Al ions in the alumina structure. However, the differences are within the estimated error range. Furthermore, the attempts to refine the electron density in the octahedral site – assuring the convergence of isotropic displacement parameters – suggest the only presence of aluminium ions.

3.3. X-ray photoelectron and diffuse reflectance spectroscopy

All the three tested samples showed XPS spectra characterised by two Mo(VI) peaks centred at 232.2 and at 235.7 eV, respectively (Fig. 4). Interesting enough, the intensity ratio of the Mo and Al peaks is perfectly correlated with the MoO_3 content measured by ICP-OES (Table 1). Similar XPS spectra were collected by other authors [7,11,13]: there was no evidence for Mo (IV) or Mo (V) in molybdenum films over α-Al_2O_3, even when strongly reducing conditions were applied. Though the width of $Mo3d_{5/2}$ peaks was used as a clue for the occurrence of multiple valences (e.g. FWHM values around 2.7 eV [13]), it depends mainly on the thickness of the molybdena film [7]. In our pigments these FWHM values are about 1.8 eV, therefore corresponding to ≅1% Mo loading according to Spevack and McIntyre [7] in good accordance with our ICP data.

The diffuse reflectance spectra are characterised by a conspicuous light absorption in the UV–vis–NIR range,

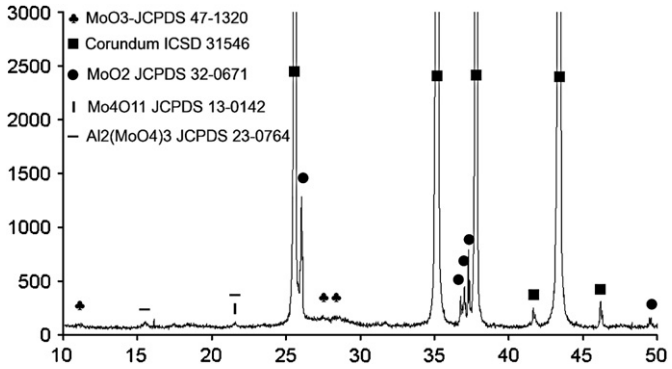

Fig. 2. X-ray powder diffraction pattern of sample AM15.

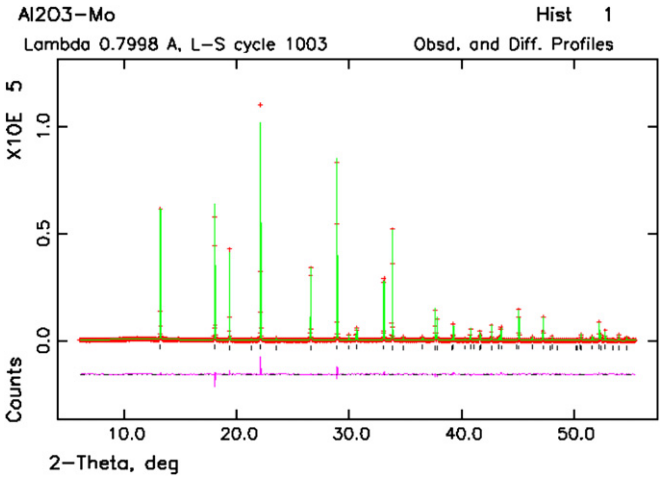

Fig. 3. Rietveld refinement plot of the X-ray powder diffraction data of the sample AM8. In the figure the continuous line represents the calculated pattern, while cross points show the observed pattern. The difference curve between observed and calculated profiles is plotted below.

where two very broad humps are clearly distinguished (Fig. 5) being separated by a minimum of absorbance in between 22,000 and 25,000 cm^{-1}, corresponding to 400–450 nm, thus explaining the blue shade perceived by the human eye. These spectra are very similar to those obtained for the same system by Siokou and co-workers [13].

The two above-mentioned humps were successfully deconvolved assuming the occurrence of mainly crystal field (CF) electronic transitions at lower energies (i.e. <22,000 cm^{-1}) and oxygen-metal charge transfer (MLCT) at the higher wavenumbers, in agreement with the known optical response of molybdenum-bearing oxides [13,22].

In particular, three CF transitions were found (Table 2):

- A weak band below 10,000 cm^{-1} (υ_1) rather steady in all samples; being far in the infrared, it has little or no influence on coloration.
- An intense peak centred at about 12,000 cm^{-1} (υ_2); being extended also in the red–orange region of the visible range, it is mainly responsible for the blue shade of pigments.

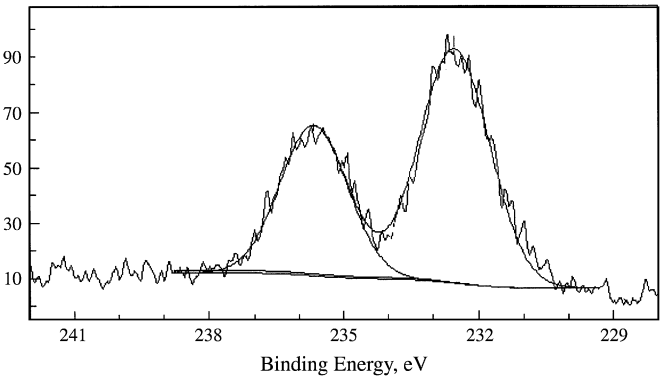

Fig. 4. X-ray photon spectroscopy Mo(3d) spectrum of pigment AM10.

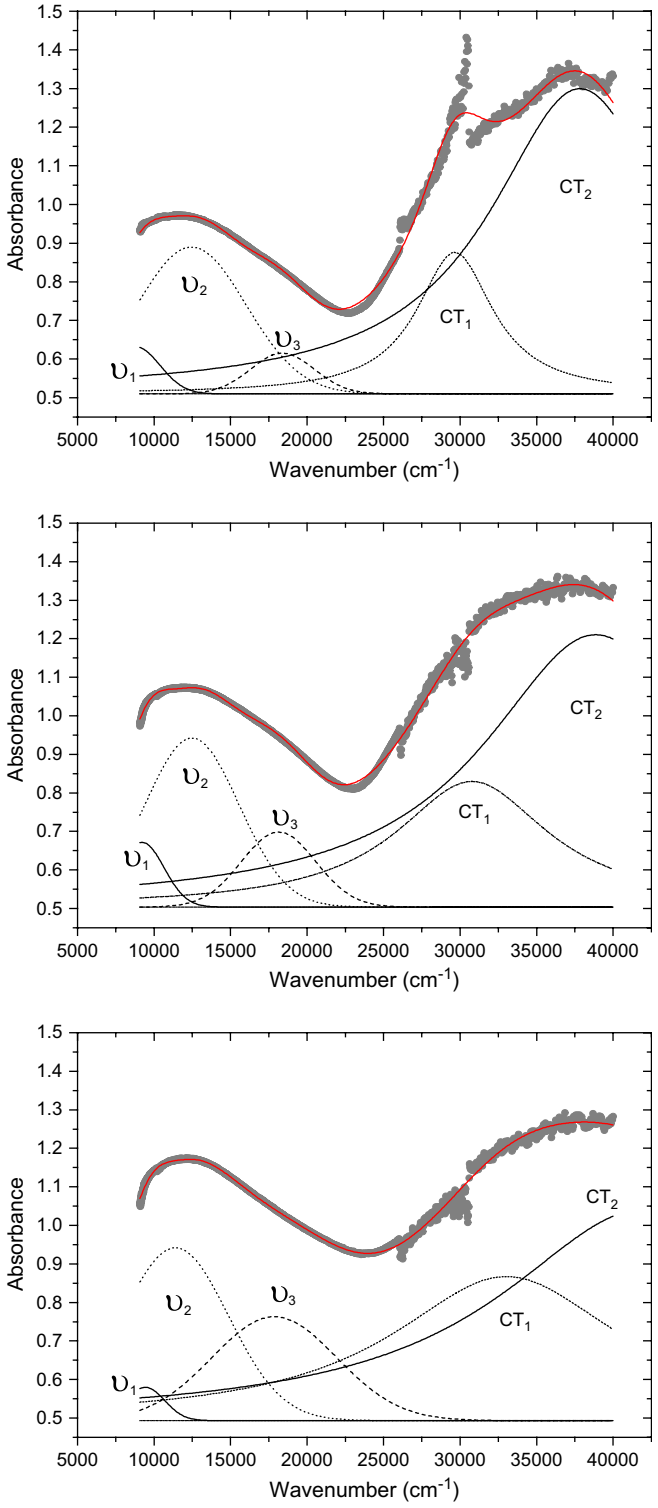

Fig. 5. Diffuse reflectance spectroscopy of the alumina–molybdena pigments (from top to bottom sample AM8, AM10, AM15, respectively). Spectra are deconvolved in three Gaussian bands (υ_1, υ_2 and υ_3, crystal field transitions) and two Lorentzian bands (CT_1 and CT_2, charge transfer).

– A quite broad band at approximately 18,000 cm^{-1} (υ_3), thus absorbing much of the yellow and green wavelengths; even if its intensity is growing from AM8 to AM15, it provokes just the above-mentioned shift in the minimum of absorbance.

These electronic transitions can be assigned to either Mo(V) or Mo(IV) ions, as Mo(VI) gives absorptions only far in the UV range (>40,000 cm^{-1}) [22]. Mo(V) has the electronic configuration d^1, for which the single transition $^2T_{2g}(^2D) \rightarrow {}^2E_g(^2D)$ is expected, but a remarkable splitting is usually observed in several complexes, leading to two absorptions at 13,000–15,000 cm^{-1} and 19,000–23,000 cm^{-1}, respectively [22]. The former can be reasonably shifted to slightly lower energies (e.g., ~12,500 $cm^{-1} = \upsilon_2$) because of the presumably strong distortion of $[MoO_6]$ polyhedra spread over the alumina surface; the latter band is superimposed by MLCT and cannot be resolved in the alumina–molybdena pigments. The intensity of this υ_2 band appears to be somewhat too high for a parity-forbidden transition, even accounting for a contribution at low wavenumbers by the tail of any MLCT broad band. Thus, some Mo(IV)–Mo(V) intervalence charge transfer (IVCT) cannot be excluded, though this kind of transition is not usually claimed for the Al_2O_3–MoO_x system.

The electronic configuration d^2 of Mo(IV) implies two main CF bands: $^3T_1(^3F) \rightarrow {}^3T_2(^3F)$ and $^3T_1(^3F) \rightarrow {}^3T_1(^3P)$ that in molybdenum compounds are generally found at 18,000–22,000 cm^{-1} and 25,000–28,000 cm^{-1}, respectively [22–24]. The υ_3 peak at ~18,000 cm^{-1} is consistent with the $^3T_2$ transition, while the $^3T_1(^3P)$ one falls in the MLCT field [22].

The υ_1 band does not match any expected electronic absorption neither for Mo(IV) nor for Mo(V). Nevertheless, a low energy peak at ~10,500 cm^{-1} – hence not so far from υ_1 (~9300 cm^{-1}) – is assigned to a $^1B_1 \rightarrow {}^1A_1$ weak transition of molybdenum in tetrahedral coordination or in Mo_4O_{11} [22,25].

Interesting enough, the υ_2 and υ_3 bands exhibit different trends of their intensity as function of molybdena concentration. In particular, the υ_3 peak is distinguished by a strong growth; in contrast, the υ_2 intensity is almost constant (Fig. 6). This circumstance suggests a fast increase of Mo(IV), while the concentration of Mo(V) remains to a large extent steady passing from AM8 to AM15.

The formation of the lower valences of molybdenum has been attributed to oxygen vacancies that are thought to capture one or two electrons from cationic orbitals, thus giving rise to Mo(V) and Mo(IV) ions, respectively. These colour centres entrap free electrons in the oxygen vacancies, being already intensely active below 400 °C [13].

The spectrum at the higher energies was deconvolved by a couple of very broad Lorentzian bands, consistent with charge transfer between Mo and O orbitals, whose assignment is so insecure that little gain is expected by a detailed interpretation [22].

3.4. Colouring performance

Alumina–molybdena pigments exhibit a deep grayish-blue colour that has no analogue among ceramic pigments [15]. Their peculiar blue shade (i.e. $-6 < b^* < -8$), however, is much less intense than that of cobalt aluminate or V-doped

Table 2
Optical spectroscopy data of alumina–molybdena pigments

Band	Parameter	Unit	AM8	AM10	AM15
υ_1 (Gaussian)	Centre max	cm^{-1}	8820	9220	9440
	FWHM	cm^{-1}	3710	3390	2950
	Max height	K/S	.122	.168	.086
	Fitted area	a.u.	480	610	270
υ_2 (Gaussian)	Centre max	cm^{-1}	12,460	12,480	11,390
	FWHM	cm^{-1}	8400	7250	8180
	Max height	K/S	.380	.438	.448
	Fitted area	a.u.	3390	3380	3900
υ_3 (Gaussian)	Centre max	cm^{-1}	18,400	18,140	17,860
	FWHM	cm^{-1}	4920	5720	9610
	Max height	K/S	.105	.194	.269
	Fitted area	a.u.	550	1180	2760
CT_1 (Lorentzian)	Centre max	cm^{-1}	29,660	30,780	33,030
	FWHM	cm^{-1}	6070	12,130	18,330
	Max height	K/S	.366	.326	.373
	Fitted area	a.u.	3500	6200	10,800
CT_2 (Lorentzian)	Centre max	cm^{-1}	37,830	38,860	42,090
	FWHM	cm^{-1}	14,380	17,890	22,910
	Max height	K/S	.789	.707	.548
	Fitted area	a.u.	17,800	19,900	19,700

zircon (Table 3). Nevertheless, the peculiar coloration imparted by Al_2O_3–MoO_x pigments cannot be reproduced with available ceramic colorants, unless using blue and black cobalt spinels, which are at large the most expensive in the market [15].

The colouring performance was tested dispersing the alumina–molybdena pigments into a porcelain stoneware body and three ceramic glazes for floor tiles that underwent a typical industrial firing in roller kilns, implying high temperature (1150–1220 °C) and fast cycles (45–60 min cold-to-cold). The oxygen-deficient kiln atmosphere – made up of flue gas from burners fed with a nearly stoichiometric methane–air mixture – fostered the development of an intense grayish-blue coloration that in the glazes preserved a blue component substantially equivalent to that of the pigment (Table 3). The parameter b^* is slightly reduced in the body, because of interference with the relevant yellow component of porcelain stoneware (i.e. $b^* \sim 10$).

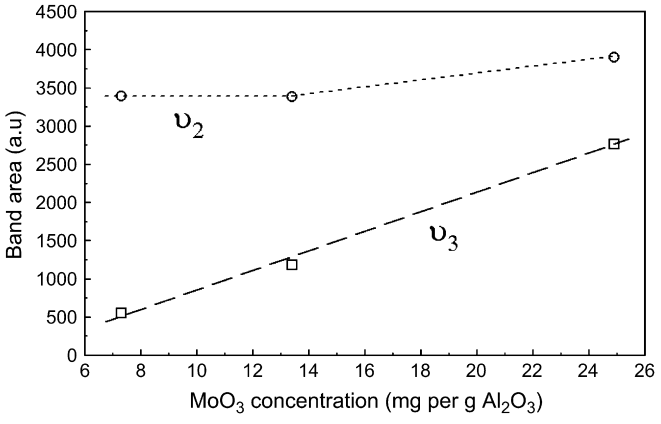

Fig. 6. Intensity of the Mo(IV) and Mo(V) electronic transition bands as function of the amount of molybdenum oxide in the pigment.

In order to get insights on which chemical components of ceramic matrices most affect the colouring performance, the Al_2O_3–MoO_x pigments were further tested in six different glazes and glassy coatings, representing a wide range of firing temperatures (950–1300 °C in oxidising atmosphere) and ceramic applications (wall and floor tiles, sanitary ware). The degree of thermal stability was expressed by the change of blue colour with respect to the pigment: i.e. the b^*_g/b^*_p ratio, where the CIE blue parameter is referred to the ceramic ware (b^*_g) or the pigment (b^*_p). This colour ratio resulted to be lower in laboratory-fired samples with respect to industrial firing; this behaviour is probably due – together with the different kiln atmosphere – to the very thin layer of glaze or glassy coating applied in laboratory testing. An effect of temperature arises once comparing the same coating after different firings; the certain drop of blue intensity occurring at increased temperature, however, is not always significant and often it is lower than the differences between the several ceramic matrices (Fig. 7).

The complex influence exerted by the variable chemical environment of glazes and glassy coatings was appraised through a multivariate statistical analysis. The extraction of principal components gave three significant factors, accounting on the whole for 78.5% of the total variance (Fig. 8). This statistical tool allows a qualitative interpretation of relationships among variables; with reference to the inset of Fig. 8, it can be inferred that the variable A is directly related to variable B, inversely related to variable C, and has no significant relationship with variable D [26]. From this standpoint, the thermal stability of alumina–molybdena pigments being directly proportional with the colour ratio

Table 3
Colour of alumina–molybdena pigments and industrial blue ceramic pigments

Ceramic pigment	State	CIELab parameters			Note
		L^*	a^*	b^*	
AM8	Powder	36.5	−1.5	−6.2	
AM10	Powder	40.5	−1.3	−8.4	
AM15	Powder	45.4	−1.8	−7.9	
AM10	Glaze G1	42.8	−1.3	−7.9	Porcelain stoneware
AM10	Glaze G2	63.3	−1.9	−7.2	Light-coloured stoneware
AM10	Glaze G3	51.1	−1.5	−7.6	Light-coloured stoneware
AM10	Body PS	44.4	−2.3	−4.6	Porcelain stoneware
$CoAl_2O_4$	Glaze	–	+2 ÷ +10	−16 ÷ −28	[15]
V–$ZrSiO_4$	Glaze	–	−8 ÷ −12	−10 ÷ −25	[15]
$(Zn,Co)_2SiO_4$	Powder	40 ÷ 55	+2 ÷ +4	−2 ÷ −20	[16]

BR (b^*_g/b^*_p), it appears that the chemical components that mostly contribute to the loss of colouring performance are Na_2O and MgO. Interestingly, some components that are usually considered strongly aggressive for ceramic pigments – such as B_2O_3, BaO, CaO, PbO and ZnO [15] – seem to have a negligible effect on the Al_2O_3–MoO_x system.

4. Conclusions

New ceramic pigments with a deep grayish-blue coloration were obtained calcining Al_2O_3–MoO_3 mixtures at high temperature in a reducing atmosphere. We are dealing with a new kind of mordant or chemi-adsorbed pigments, as molybdenum does not substitute aluminium in the corundum lattice, but it is diffused on the alumina surface in high concentrations, ranging from 27 to 99 Mo atoms nm^{-2}, depending on the initial Al/Mo ratio. These values are largely exceeding the dispersion limit of molybdenum over α-Al_2O_3, implying a prevailing octahedral coordination of Mo ions and a certain long-range order, witnessed by the formation of crystalline MoO_2 in the sample richest in molybdenum.

Spectroscopic results indicate that pigments are mixed valent, Mo(VI) being predominant over Mo(V) and Mo(IV); the latter seems to increase its concentration with decreasing Al/Mo ratio. The colouring mechanism mostly consists of a selective absorption of the red–orange light by a crystal field transition of Mo(V), with a possible contribution by Mo(IV)–Mo(V) intervalence charge transfer, resulting in a characteristic blue shade. The strong light absorbance over the entire UV–vis–NIR range, responsible for the gray cast, is attributable to Mo–O charge transfer and also crystal field electronic absorptions of Mo(IV).

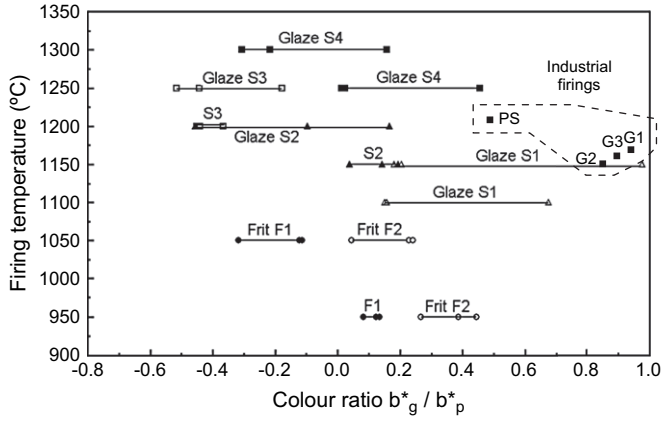

Fig. 7. Thermal stability of alumina–molybdena pigments in different ceramic glazes and glassy coatings expressed in terms of the b^*_g/b^*_p ratio, i.e. blue component of glaze/glassy coating (b^*_g) and pigment (b^*_p).

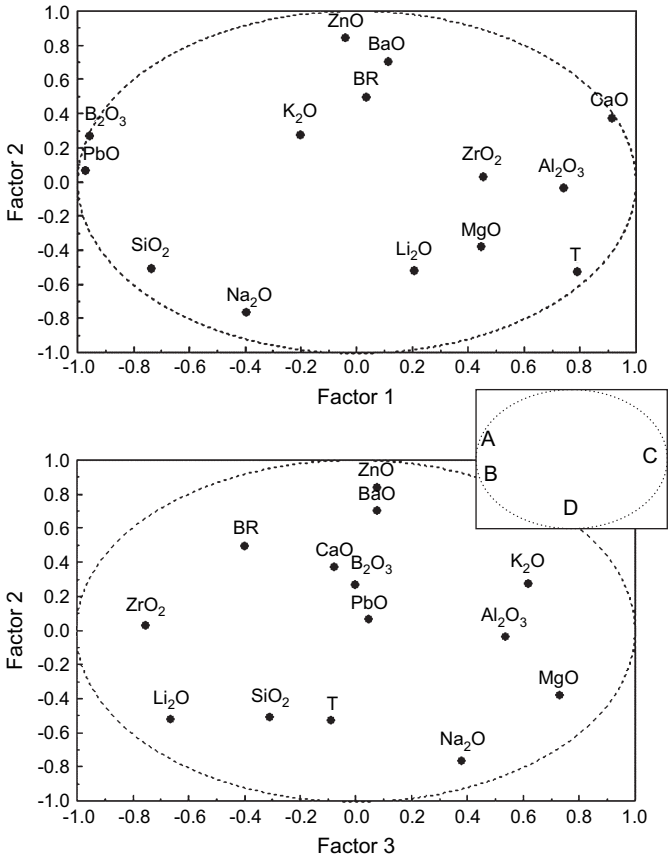

Fig. 8. Factorial analysis of the technological behaviour of alumina–molybdena pigments in ceramic glazes and glassy coatings. The extraction of principal components gave three significant factors, explaining 78.5% of the total variance. BR = b^*_g/b^*_p, T = temperature. See text for explanation of relationships among variables (inset).

The Al_2O_3–MoO_x behaves satisfactorily into porcelain stoneware bodies as in ceramic glazes for floor tiles, being the colouring performance analogue to that of the pure pigment. This excellent stability at high temperature (1150–1220 °C) could be promoted by the oxygen-deficient atmosphere of industrial kilns, as the coloration tested in an oxidant environment (i.e. electric kiln) proved to be less stable, though mostly affected by the occurrence of Na_2O and MgO into the ceramic coatings where the pigment is dispersed.

Even if the colour of alumina–molybdena pigments ($-8 < b^* < -6$) is much less blue than that of current industrial pigments, their peculiar grayish-blue shade cannot be reproduced, unless using very expensive colorants based on cobalt oxide.

Acknowledgements

Authors are grateful to ESRF for providing access to synchrotron radiation under the public beamtime programme (exp. No. CH1321). Many thanks to Dr. Maria Chiara Dalconi, Guia Guarini and Dr. Andrea Ruffini for their useful assistance in the XRPD, BET and ICP-OES analyses, respectively.

References

[1] Haber J. The role of molybdenum in catalysis. Ann Arbor, MI: Climax Molybdenum Co.; 1981.
[2] Zi F, Yang J, Yan P, Wang X, Guo H, Wu N. J Mater Chem 2003;13:1206–9.
[3] Sarrazin P, Kasztelan S, Payen E, Bonnelle JP, Grimblot J. J Chem Phys 1993;97:5954–61.
[4] Hu H, Wachs IE, Bare SR. J Phys Chem 1995;99:10897–910.
[5] Günther S, Gregoratti L, Kiskinova M, Taglauer E, Grotz P, Schubert UA, et al. J Chem Phys 2000;112(12):5440–6.
[6] Xu W, Yan J, Wu N, Zhang H, Xie Y, Tang Y, et al. Surf Sci 2000;470:121–30.
[7] Spevack PA, McIntyre NS. J Phys Chem 1993;97:11020–30.
[8] Reddy BM, Chowdhury B, Reddy EP, Fernàndez A. Appl Catal A Gen 2001;213:279–88.
[9] El-Shobaky HG, Mokhtar M, Ahmed AS. Thermochim Acta 1999;327:39–46.
[10] El-Shobaky GA, Abdalla FHA, Ghozza AM, Khalil KA. Thermochim Acta 1996;275:235–347.
[11] Plyuto YuV, Babich IV, Plyuto IV, Van Langeveld AD, Moulijn JA. Appl Surf Sci 1997;119:11–8.
[12] Sarrin J, Noguera O, Royo H, Perez Zurita MJ, Scott C, Goldwasser MR, et al. J Mol Catal A Chem 1999;144:441–50.
[13] Siokou A, Lefheriotis G, Papaefthimou S, Yianoulis P. Surf Sci 2001;482–485:294–9.
[14] Larrubia MA, Busca G. Mater Chem Phys 2001;72:337–46.
[15] Eppler RA. Am Ceram Soc Bull 1987;66:1600–4.
[16] Fores A, Llusar M, Badenes JA, Calbo J, Tena MA, Monros G. Green Chem 2000;2(3):93–100.
[17] Larson AC, Von Dreele RB. Los Alamos National Labaratory Report LAUR 86-748; 2000.
[18] Toby BH. J Appl Crystallogr 2001;34:210–3.
[19] Maslen EN, Strel'tsov VA, Strel'tsova NR, Ishizawa N, Satow Y. Acta Crystallogr B 1993;49:973–80.
[20] Matteucci F, Lepri Neto C, Dondi M, Cruciani G, Baldi G, Boschi AO. Adv Appl Ceram 2006;105:99–106.
[21] Cox DE, Moodenbaugh AE, Sleight AW, Chen H-Y. National Bureau of Standards (U.S.), Special Publication, vol. 567; 1980. p. 189–201.
[22] Lever ABP. Inorganic electronic spectroscopy. 2nd ed. Amsterdam: Elsevier; 1984.
[23] Carmichael WM, Edwards DA, Walton RA. J Chem Soc A 1966;97.
[24] Chisholm MH, Cotton FA, Extine MW. Inorg Chem 1978;17:1329.
[25] Porter VR, White WB, Roy R. J Solid State Chem 1972;4:250–4.
[26] Cooley WW, Lohnes PR. Multivariate data analysis. New York: Wiley; 1971.